Biochimica et Biophysica Acta 1837 (2014) 1490–1499

Contents lists available at ScienceDirect

Biochimica et Biophysica Acta

journal homepage: www.elsevier.com/locate/bbabio

Excitation energy transfer and electron-vibrational coupling in phycobiliproteins of the cyanobacterium *Acaryochloris marina* investigated by site-selective spectroscopy ☆

G. Gryliuk [a], M. Rätsep [a], S. Hildebrandt [b], K.-D. Irrgang [b], H.-J. Eckert [c], J. Pieper [a,*]

[a] Institute of Physics, University of Tartu, Tartu, Estonia
[b] Department of Life Science & Technology, Laboratory of Biochemistry, University for Applied Sciences, Berlin, Germany
[c] Max-Volmer-Laboratories for Biophysical Chemistry, Technical University Berlin, Germany

ARTICLE INFO

Article history:
Received 2 December 2013
Received in revised form 26 January 2014
Accepted 12 February 2014
Available online 21 February 2014

Keywords:
Acaryochloris marina
Phycobiliproteins
Excitation energy transfer
Electron phonon coupling
Spectral hole-burning
Difference fluorescence line-narrowing

ABSTRACT

In adaption to its specific environmental conditions, the cyanobacterium *Acaryochloris marina* developed two different types of light-harvesting complexes: chlorophyll-d-containing membrane-intrinsic complexes and phycocyanobilin (PCB) — containing phycobiliprotein (PBP) complexes. The latter complexes are believed to form a rod-shaped structure comprising three homo-hexamers of phycocyanin (PC), one hetero-hexamer of phycocyanin and allophycocyanin (APC) and probably a linker protein connecting the PBPs to the reaction centre. Excitation energy transfer and electron-vibrational coupling in PBPs have been investigated by selectively excited fluorescence spectra. The data reveal a rich spectral substructure with a total of five low-energy electronic states with fluorescence bands at 635 nm, 645 nm, 654 nm, 659 nm and a terminal emitter at about 673 nm. The electronic states at ~635 and 645 nm are tentatively attributed to PC and APC, respectively, while an apparent heterogeneity among PC subunits may also play a role. The other fluorescence bands may be associated with three different isoforms of the linker protein. Furthermore, a large number of vibrational features can be identified for each electronic state with intense phonon sidebands peaking at about 31 to 37 cm^{-1}, which are among the highest phonon frequencies observed for photosynthetic antenna complexes. The corresponding Huang-Rhys factors S fall in the range between 0.98 (terminal emitter), 1.15 (APC), and 1.42 (PC). Two characteristic vibronic lines at about 1580 and 1634 cm^{-1} appear to reflect C – NH^+ and C – C stretching modes of the PCB chromophore, respectively. The exact phonon and vibrational frequencies vary with electronic state implying that the respective PCB chromophores are bound to different protein environments. This article is part of a Special Issue entitled: Photosynthesis Research for Sustainability: Keys to Produce Clean Energy.

1. Introduction

Photosynthetic organisms have developed highly specialized antenna pigment–protein complexes for efficient light harvesting and excitation energy transfer (EET) [1,2] to reaction centre (RC) complexes, where primary charge separation and secondary electron transfer take place. Eventually these processes lead to water oxidation under release of oxygen and formation of the energy rich compounds ATP and NADPH (for a review see Blankenship and Govindjee [3]).

In contrast to other oxygenic photosynthetic organisms, the cyanobacterium *Acaryochloris marina* (*A. marina*) contains Chlorophyll (Chl) *d* as the dominant photosynthetic pigment [4]. The Q_y absorption band of Chl *d* in organic solvents is shifted to the red by more than 30 nm in comparison with Chl *a*. This enables *A. marina* to exploit far red light above 700 nm in habitats with largely reduced visible light e.g. underneath a sea squirt [4,5] which contains a thick layer of the Chl a/b containing prochlorophytes *Prochloron didemni* [4,5].

The antenna system of *A. marina* (strain MBIC 11017) comprises the core light-harvesting complexes CP43/CP47, the membrane internal Prochlorophyte Chl *d* binding proteins [6,7] and the membrane external phycobiliprotein (PBP) complexes [8,9]. As to the latter, PBP complexes exhibit a broad absorption band around 618 nm at room temperature enabling them to utilize also the visible light in the "green gap" between 500 nm and 650 nm, which is outside of the main absorption range of Chls [8,9]. The PBSs are located on the cytoplasmic side of *A. marina*

Abbreviations: APC, allophycocyanin; Chl, Chlorophyll; EET, excitation energy transfer; FLN, fluorescence line-narrowing; ΔFLN, difference fluorescence line-narrowing; FWHM, full width at half maximum; IDF, inhomogeneous distribution function; PC, phycocyanin; PBP, phycobiliprotein; PBS, phycobilisomes; PCB, phycocyanobilin; PE, phycoerythrin; PSB, phonon sideband; RC, reaction centre; SHB, spectral hole-burning; ZPL, zero-phonon line

☆ This article is part of a Special Issue entitled: Photosynthesis Research for Sustainability: Keys to Produce Clean Energy.

* Corresponding author at: Institute of Physics, University of Tartu, Riia 142, 51014 Tartu, Estonia. Tel.: +372 737 4627; fax: +372 738 3033.
E-mail addresses: irrgang@beuth-hochschule.de (K.-D. Irrgang), pieper@ut.ee (J. Pieper).

http://dx.doi.org/10.1016/j.bbabio.2014.02.010
0005-2728/

between non-appressed regions of the thylakoid membranes [10,11] and they are arranged in unique near-crystalline arrays that can occupy up to 50% of the stromal surface of the thylakoid [11]. In contrast to other cyanobacteria, PBPs of *A. marina* (strain MBIC 11017) are organized in rod-like structures that were suggested to consist of three hexamers containing phycocyanin (PC) and a further hetero-hexamer containing PC and allophycocyanin (APC) [8]. From the APC-containing hetero-hexamer the excitation energy appears to be directly funnelled to Chl *d* of PS II [9,12]. Thus, the PBP complexes of *A. marina* have a much simpler structure than the phycobilisomes (PBS) in common Chl *a*-containing cyanobacteria which consist of an APC-containing core complex, and usually six rod-like structures formed by either PC-hexamers or both PC- and phycoerythrin (PE) — hexamers. (see [13–15] for reviews). The main room-temperature absorption bands of PE, PC and APC are located at 560–575 nm, 618 nm, and 652 nm, respectively. Thus, the physical arrangement of PBP with the lowest energy trimer (APC) lying close to the thylakoid membrane is a prerequisite for efficient downhill EET to the chlorophylls of PS II [13].

Transient absorption experiments with femtosecond (fs) resolution [16] revealed a complex EET dynamics in the PBP antenna of *A .marina*. Upon excitation at 618 nm, fast sub-picosecond EET from ~620 nm to ~630 nm is followed by slower EET to states at ~640 nm and eventually to the terminal emitter at ~670 nm [16].

In order to achieve a detailed understanding of EET in PBP of *A. marina*, the results of time-resolved spectroscopy have to be supplemented by investigations of spectral positions and excitonic nature of excited electronic states as well as of electron-vibrational coupling. However, due to the amorphous nature of pigment–protein complexes, such spectral substructures are typically hidden by significant inhomogeneous broadening even at low temperature (for reviews see Purchase and Völker [17], Jankowiak et al. [18]). Site-selective spectroscopies like spectral hole-burning (SHB) [17,18], fluorescence line-narrowing (FLN), and difference fluorescence line-narrowing (ΔFLN) [19–21] are efficient experimental tools to circumvent inhomogeneous broadening and to obtain parameters of homogeneously broadened spectra. Resonant SHB has been used to measure pure dephasing times T_2 [22–24] and excited state lifetimes T_1 [25,26]. In addition, constant fluence or action spectroscopy reveals the inhomogeneous distribution function (IDF) of the lowest energy states of a given pigment-protein complex [22,24,25,27–30]. Information on electron–phonon [31–35] and electron-vibrational [36,37] coupling can be gathered from non-resonant vibrational satellite holes. In case of vibrational spectroscopy, SHB has recently been supplemented by the complementary ΔFLN spectroscopy [19–21,38–40]. Briefly, a ΔFLN spectrum is obtained as the difference between two FLN spectra recorded before and after spectral hole burning [19–21]. In contrast to "conventional" FLN, this subtraction technique provides a zero-phonon line (ZPL) virtually free from scattering artefacts of the excitation laser beam so that electron-phonon as well as electron-vibrational coupling strengths can be directly determined [21,39]. SHB has already been applied to investigate cyanobacterial PE [41], PC [42,43] and APC [42]. However, detailed studies on PBP of *A. marina* using site selective spectroscopy are so far lacking.

In the present study, we apply ΔFLN spectroscopy for an investigation of excited state positions as well as electron–phonon and electron-vibrational coupling of PBP isolated by sucrose density gradient fractionation as described in ref. [8] with minor modifications. The results obtained provide valuable information for a further understanding of EET in the PBP antenna of *A. marina*, which are complementary to those of time-resolved experiments mentioned above.

2. Materials and methods

2.1. Sample preparation

Cells of *A. marina* (MBIC-11017) were grown in artificial sea water containing iron at a concentration of 2 mg/L at 6–10 μE (m^2s) as described in Ref. [44]. Phycobiliproteins were isolated and purified by density gradient centrifugation using a linear sucrose gradient (15–35% (w/v) sucrose in 750 mM potassium phosphate buffer, pH 7.2, 2 mM EDTA, 0.05% (w/v) N,N-Dimethyldodecylamine N-oxide (LDAO)) with some modifications as described by Marquardt et al. [8]. Solubilization of phycobiliproteins was carried out for 40 min with LDAO using a detergent to chlorophyll ratio of 20.6/1 (w/w) at room temperature (final amount of LDAO: 1.5% (w/v)). The samples were centrifuged for 16 h at 41,000 rpm in a VTi 50 rotor at 4 °C. After running, the centrifugation tubes were punctured from the bottom. Fractions collected were concentrated using Centricon 10 tubes at 3000 rpm and characterized by absorption spectroscopy at room temperature and the calculated second derivative spectra. Protein compositions were analyzed by SDS-PAGE [45] in the absence or presence of dithiothreitol. Staining of proteins was either performed with colloidal Coomassie G 250 or with silver nitrate (PAGE silver staining kit, Fermentas GmbH) [46]. Furthermore, phycobiliproteins were detected in gel after incubation of the polyacrylamide gels with $ZnSO_4$ [47]. Fluorescent bands were identified using a Luminescent Image Analyzer Las 4000 (Fujifilm). Samples were excited at 312 nm and emission was detected using an orange filter at <605 nm. After in gel digestion of electrophoretically separated proteins with trypsin phycobiliproteins and phycobilisome linker proteins were identified by nano-liquid chromatography (LC)–electrospray ionization (ESI)–mass spectrometry in combination with genomic sequence data published by Swingley et al. [48] and Mascot data bank searching (data not shown). Phycobilin concentrations were calculated using the formulae reported in Rowan [49]. Chl d and Chl a were quantitatively analyzed in 100% methanol at 696 and 665 nm, respectively following Ritchie [50]. The samples were dissolved in a glass-forming buffer solution containing 0.75 M K_2HPO_4 and KH_2PO_4 at pH = 7.0, 2 mM EDTA, and 70% (w/v) glycerol.

2.2. Experimental setup

Low-temperature absorption measurements were carried out using a Perkin Elmer Lambda 9 spectrometer and an Oxford Optistat CF-V cryostat. The setup for hole burning and fluorescence line-narrowing has been described in ref. [51]. Briefly, a Spectra Physics model 375 dye laser with a linewidth of <0.5 cm^{-1} pumped by a solid state laser (Spectra Physics, USA) was used as the burn laser. Transmission and fluorescence measurements employed a high stability tungsten light source BPS100 (B&W Tek, USA) and a 0.3 m spectrograph (Shamrock SR-303i, Andor Technology, UK) combined with an electrically cooled CCD camera (DV420A-OE, Andor Technology, UK) operated at a resolution of 0.4 nm. A He-bath cryostat (Utreks, Ukraine) was employed to control the sample temperature.

2.3. Data analysis

The ΔFLN spectrum in the short burn time limit is widely identical to the homogeneously broadened fluorescence spectrum [19,20,52] which for several phonon modes (k) and arbitrary temperature takes the form [53]

$$L(\omega) = e^{-\sum_k S_k(2\overline{n}_k+1)} \prod_k \sum_{R=0}^{\infty} \sum_{r=0}^{R} \frac{[S_k(\overline{n}_k+1)]^{R-r}[S_k\overline{n}_k]^r}{(R-r)!r!} \times l_{R,r}\left[\omega-\Omega_0 \mp \sum_k (R-2r)\omega_k\right] \quad (1)$$

where S_k is the electron–phonon coupling strength (Huang–Rhys factor), $l_{1,0}$ is the one-phonon profile (now often referred to as the spectral density), and $\overline{n}_k = [\exp(\hbar\omega_k/kT)-1]^{-1}$ describes the thermal occupation for phonons of mode k according to Bose statistics and - and + correspond to absorption and fluorescence, respectively. All transitions with R = 0

correspond to zero-phonon transitions constituting the ZPL at the electronic transition energy. The value of R (with R = 1,2,…) denotes the total number of phonon transitions, while r gives the number of annihilated phonons ($0 \le r \le R$). Therefore, all transitions with $R > 0$ form the phonon sideband (PSB). The profile $I_{R,r}$ ($R > 1$) is obtained by folding the one-phonon profile $I_{1,0}$ |R-2r|-times with itself. Here, we employ a one-phonon profile composed of a Gaussian and a Lorentzian shape at its low- and high-energy wings, respectively.

3. Results

First we will discuss the non-line-narrowed spectra of PBP complexes of *A. marina* presented in Fig. 1. The room temperature (293 K) absorption spectrum of PBP complexes of *A. marina* (see dashed black curve in Fig. 1) is widely structure less with a major peak at ~619 nm and a pronounced shoulder at ~585 nm. At 4.5 K the absorption spectrum of PBPs exhibits three discernible peaks at ~574, ~599 and ~629 nm (see black curve in Fig. 1). These peaks agree well with those observed in previous measurements on PC of common cyanobacteria [42] and with those of PC from *A. marina* [9]. Furthermore, the absorption spectrum exhibits a weak shoulder at ~645 nm and a long tailing towards longer wavelengths. Despite of a different spectral position than observed in ref. [42], the shoulder at ~645 nm can most probably be attributed to APC. Note that in the latter work a small amount of APC was present in the PC sample. In the present work, we are reporting on the rod-shaped PBP antenna from *A. marina*, which contains both, PC and APC. The spectral features are better visible in the second derivative of the absorption spectrum shown as a red curve in Fig. 1. Three minima are almost coincident with the absorption peaks mentioned above, while a further minimum at 644.5 nm provides support for the presence of a corresponding subband. The 4.5 K fluorescence spectrum is shown as a blue line in Fig. 1 and reveals a major peak at ~645 nm and a pronounced shoulder at ~636 nm. The latter features are also visible as minima in the corresponding second derivative spectrum (see dashed blue line in Fig. 1). Tentatively, it can be assumed that the fluorescence peak at 636 nm originates from the absorption band at 629 nm, while the fluorescence peak at 645 nm may stem from the absorption band at 644.5 nm. Because of the strong spectral overlap of the latter two fluorescence bands, this data set does not allow for a precise assignment of the fluorescence origin. Nevertheless, a minimum of two emitting states has to be assumed. The further structure to the red of the two main fluorescence peaks is more complex. In this region fluorescence from vibrational satellite bands may be superimposed on emission from electronic states within the long absorption tail at wavelengths longer than ~650 nm, see below. In summary, however, the low-temperature absorption and fluorescence spectra are quite featureless considering the complex structural composition of the PBPs with about 70 individual pigment molecules [54].

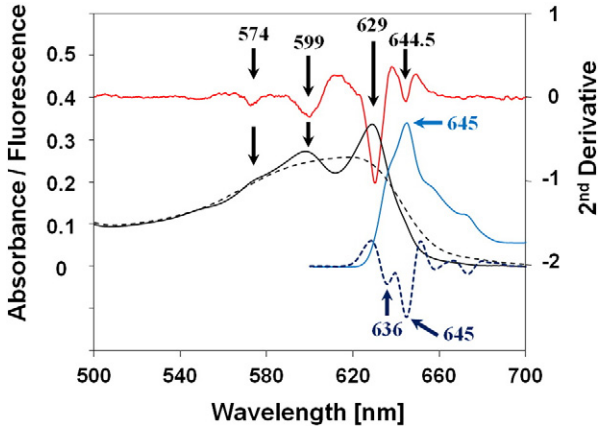

Fig. 1. 4.5 K absorption (black line) and fluorescence (blue line) spectra of PBP in a buffer solution containing 70% glycerol. The second derivatives of absorption (see right scale) and fluorescence spectra are shown as red and dashed blue lines, respectively. For comparison, the room temperature absorption spectrum is given as a dashed black line. Spectral features are labelled by their peak wavelengths in nanometer. The fluorescence spectrum was excited at 410 nm.

FLN and ΔFLN spectroscopy with several excitation wavelengths ranging from 635 to 675 nm was employed to reveal spectral substructures otherwise hidden within the inhomogeneously broadened fluorescence spectrum. Some preliminary ΔFLN data of PBPs are reported in ref. [55], however, they are presented as pure raw data without any further data analysis or coherent interpretation, whatsoever. Here we present a detailed assessment of the vibrational properties of PBP including an assignment of the vibrational modes and a calculation and verification of the electron–phonon coupling strengths of individual electronic states of PBP. Four representative sets of pre-burn FLN and ΔFLN spectra of PBPs of *A. marina* are shown in Figs. 2–5. First, an excitation wavelength of 635 nm was chosen, because it is located within the lowest absorption band of PC. The pre-burn FLN spectrum obtained at this excitation wavelength (see Fig. 2) reveals mainly three broad fluorescence bands at about 645.5, 654 and 673 nm, respectively, which still appear to be inhomogeneously broadened. In addition, the spectrum is superimposed with a large number of narrow vibrational lines. The ZPL located at the excitation wavelength is cut off for clarity in Fig. 2. As typically encountered in FLN experiments, the ZPL is contaminated with scattered laser light. Since the three observed broad fluorescence bands have not undergone any line-narrowing, they can most probably be associated with low-energy electronic states, which are populated by excitation energy transfer from the excitation wavelength. This means that the pre- burn FLN has not reached full selectivity.

In contrast, the ΔFLN spectrum obtained as the difference between FLN spectra excited at 635 nm before and after intermediate hole burning (see also Fig. 2) reveals more structure than a conventional FLN spectrum. It is clearly lacking the broad features visible in the FLN spectrum and consists mainly of a ZPL located at the excitation wavelength, a distinct PSB peaking 35 cm^{-1} to the red of the ZPL and several narrow vibrational lines indicated by thin arrows in Fig. 2. These features correspond to localized ground state ($S_1 \rightarrow S_0$) vibrational frequencies of the chromophores absorbing at 635 nm. The individual values of the ($S_1 \rightarrow S_0$) vibrational frequencies obtained within this study are listed in Table 1. As pointed out in the Introduction section, the ZPL of the ΔFLN spectrum is virtually free of laser light scatter and can thus be

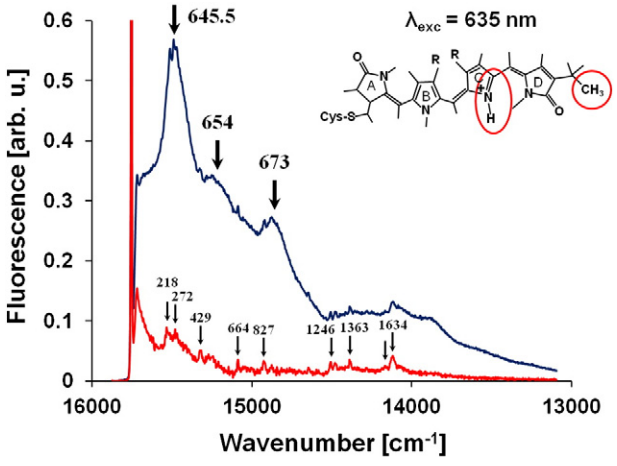

Fig. 2. Pre-burn FLN (blue) and ΔFLN spectra (red) of phycobiliproteins obtained with an excitation wavelength of 635 nm at 4.5 K. The burn fluences applied for FLN and intermediate hole burning were 1 and 25 mJ/cm^2, respectively. The read resolution was 0.4 nm. The ZPL of the ΔFLN spectrum are cut off at 60% of their peak intensity for clarity. Broad fluorescence bands unaffected by line-narrowing are labelled by bold arrows and their spectral position in wavelengths, distinct vibrational lines are marked by thin arrows and their frequencies in wavenumbers, see Table 1. The inset shows the structure of a PCB molecule following ref. [64]. The functional groups responsible for the characteristic frequencies at ~1580 and 1634 cm^{-1}, respectively, are encircled in red.

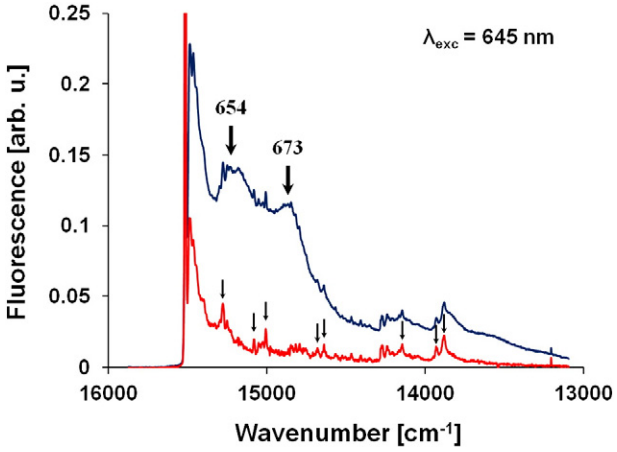

Fig. 3. Pre-burn FLN (blue) and ΔFLN spectra (red) of phycobiliproteins obtained with an excitation wavelength of 645 nm at 4.5 K. The burn fluences applied for FLN and intermediate hole burning were 1 and 25 mJ/cm^2, respectively. The read resolution was 0.4 nm. The ZPL of the ΔFLN spectrum are cut off at 25% of their peak intensity for clarity. Broad fluorescence bands unaffected by line-narrowing are labelled by arrows and their spectral position in wavelengths, distinct vibrational lines are marked by thin arrows, see Table 1.

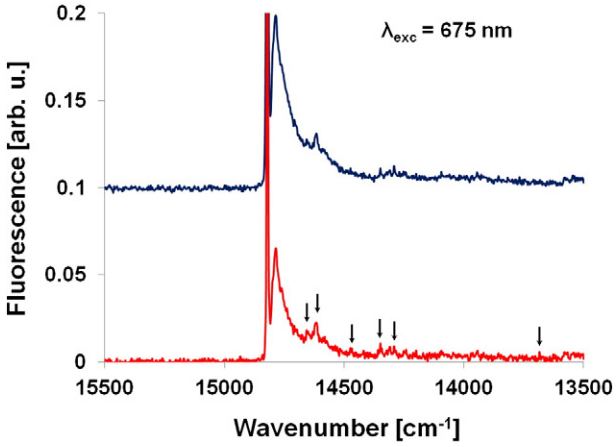

Fig. 5. Pre-burn FLN (blue) and ΔFLN spectra (red) of phycobiliproteins obtained with an excitation wavelength of 675 nm at 4.5 K. The pre-burn FLN spectrum is given an offset of 0.1 for ease of inspection. The burn fluences applied for FLN and intermediate hole burning were 1 and 25 mJ/cm^2, respectively. The read resolution was 0.4 nm. The ZPL of the ΔFLN spectrum are cut off at 13% of their peak intensity for clarity. Distinct vibrational lines are marked by thin arrows, see Table 1.

directly used to determine S factors. The overall appearance of the ΔFLN spectrum indicates that it has reached full selectivity and closely resembles the homogeneously broadened fluorescence spectrum at the excitation wavelength of 635 nm.

The pre-burn FLN spectrum obtained within the 645.5 nm-fluorescence band (see Fig. 3), which can be attributed to APC (see Discussion), shows a similar scenario as observed above with two broad fluorescence bands at about 654 and 673 nm, respectively, and a large number of distinct vibrational lines. However, the broad fluorescence band observed above at 645 nm is now lacking due to selective excitation and is replaced by the ZPL and a broad PSB peaking about 31 cm^{-1} to the red of the ZPL. Again, the ΔFLN spectrum obtained at 645 nm (see Fig. 3) is free of broad features found in the pre-burn FLN spectrum and comprises a ZPL, a distinct PSB peaking at 31 cm^{-1} and several distinct narrow vibrational replicas, which can be associated with the homogeneously broadened fluorescence spectrum at 645 nm.

The pre-burn FLN and the ΔFLN spectrum obtained at 650 nm (see Fig. 4) are very similar to the respective spectra described above with two major exceptions: a) the broad fluorescence band in the pre-burn FLN spectrum previously seen at 654 nm has shifted to 659 nm, and b)

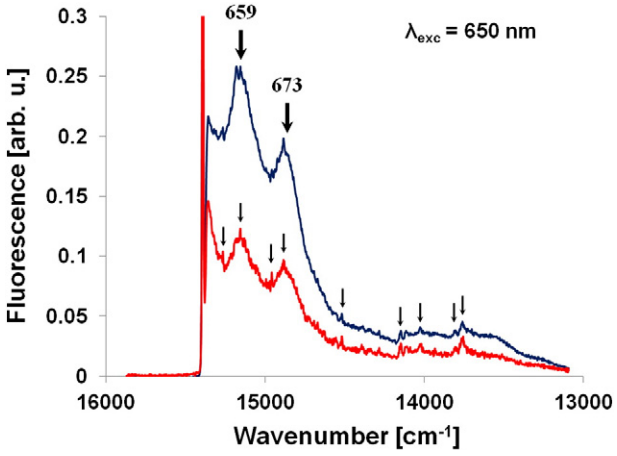

Fig. 4. Pre-burn FLN (blue) and ΔFLN spectra (red) of phycobiliproteins obtained with an excitation wavelength of 650 nm at 4.5 K. The burn fluences applied for FLN and intermediate hole burning were 1 and 25 mJ/cm^2, respectively. The read resolution was 0.4 nm. The ZPL of the ΔFLN spectrum are cut off at 30% of their peak intensity for clarity. Broad fluorescence bands unaffected by line-narrowing are labelled by arrows and their spectral position in wavelengths, distinct vibrational lines are marked by thin arrows, see Table 1.

both non-line-narrowed bands are now also visible in the ΔFLN spectrum. The first observation can most probably be explained by a weak electronic state at 659 nm, which is hidden by the intense band at 654 nm in the spectra discussed above. Once the excitation wavelength is tuned to 650 nm and beyond, the 654 nm band should be mainly selectively excited thus reducing its relative contribution to the overall spectrum and may thus reveal the weaker 659 nm band. The appearance of both broad bands in the ΔFLN spectrum suggests that there is very intense EET from the excitation wavelength to the corresponding electronic states.

Finally, at an excitation wavelength of 675 nm, the pre-burn FLN and the ΔFLN spectra (see Fig. 5) attain a highly similar shape with a ZPL and a PSB peaking at 37 cm^{-1}. The disappearance of broad features due to EET is consistent with associating the 673 nm fluorescence band with the terminal emitter.

Within the low-fluence limit, a ΔFLN spectrum yields the homogeneously broadened fluorescence spectrum so that the Huang–Rhys factor S for protein phonons can be directly obtained following Eq. (1). [19,20,52]. The phonon region, i.e. the spectral region dominated by low-frequency protein vibrations, of ΔFLN spectra measured at fluences ranging from 1 to 25.2 mJ/cm^2 is shown in Fig. 6 for the case of an excitation/burn wavelength of 635 nm. With increasing fluence, there is an increase of PSB intensity relative to the ZPL intensity concomitant with an improved signal-to-noise ratio. This increase of PSB intensity is due to a subsequent saturation of resonant hole burning and mainly of the ZPL, which leads to an increased contribution of non-resonant hole-burning favouring PSB contributions. In order to determine the Huang–Rhys factor S in the low-fluence limit, all spectra shown in Fig. 6 were fit according to Eq. (1), and the resulting S factors were plotted as a function of fluence in the inset of Fig. 6. It is apparent that the S factors increase with increasing fluence as suggested by the observed increase of PSB intensity. At fluences below 5 mJ/cm^2, however, the S factor reaches a rather constant value of ~1.42, which can thus be defined as the low-fluence limit of S. Furthermore, this simulation requires the assumption of three individual one-phonon profiles (for detailed parameters see Table 2), whose parameters were fixed by fitting the highest-fluence spectrum exhibiting the best signal-to-noise ratio. Then, the parameters of the one-phonon profiles were fixed and only the S-factors were varied to fit the remaining lower-fluence spectra. This type of approach has been repeated for all 13 excitation wavelengths between 635 and 675 nm, respectively, used in this study. The Huang–Rhys factor S and the parameters of the corresponding one-phonon profiles are compiled in Table 2. The wavelength-dependence of the S-factors is shown in Fig. 7 A along with the pre-burn FLN

Table 1
Comparison of PBP $S_1 \rightarrow S_0$ vibrational frequencies ν_j in wavenumbers [cm^{-1}] obtained by difference fluorescence line-narrowing spectroscopy at 4.5 K as a function of excitation wavelength (see first line) in this work with those of PCB in phytochrome [64] and those of Chl *a* in WSCP [65,66]. The columns corresponding to the ΔFLN spectra shown in Fig. 9 are highlighted in grey. Intense Chl *a* $S_1 \rightarrow S_0$ vibrational frequencies ν_j not observed for PBP are indicated in bold.

PCB in phytochrome (Andel et. al. [64])		635 nm	645 nm	650 nm	652.8 nm	655.3 nm	657.5 nm	660.2 nm	662.8 nm	665.2 nm	667.7 nm	670.2 nm	672.8 nm	675 nm	Chl a–WSCP from ref. 65,66 ν_j, cm^{-1}
	PSB	34	31	34	36	32	32	33	36	34	37	34	37	35	24
						210	204						202		
		218	234	237	231	240	234	241		235					228
															259
		272		267	282										283
								348							327
															356
						413		400							402
		429	432	434	432	422		429							435
					468		469	474	471	468		470	470		
493		482													481
		509	506	507	508	509	511	513	507	529	509	511	508		520
		543	536												547
		607		612		608									609
665		664	665	668	665										656
			697	700	696	706	702			708					703
762	C–H out of plane wagging modes		723	722	716	725	727	735		730	720	730	729		718
															742
801		827	834	838	841	830	826	827			826	856	842		840
873		877	877	876	876	877	874	856	858	855	878	874	874		
										873	891		902		
															920
											966	966			985
					1007	1011		1023		1034	1024	1011	1000		1024
					1052	1053	1057	1059	1064	1077	1075	1075	1060		1067
															1144
															1184
															1217
1224	C–H / N–H rocking modes	1246	1240	1245	1249	1249	1249	1243	1249	1248	1254	1242	1241 cm^{-1}	1241	1243
1295		1273	1272	1273	1282	1274	1287	1289	1286	1290	1290	1288	1289	1280	1285
1318															1329
1379		1363	1370	1366	1369	1368	1374	1373	1370	1365	1373	1374	1374	1386	1390
															1532
1571	C=NH+ stretching	1584	1583	1589	1589	1588	1595	1596	1594	1590	1591	1601	1606		1591
1634	$C_{19} - C_{20}$ stretching	1634	1634	1638	1638	1634	1638	1639	1631	1629	1629	1631	1633	1628	1620

spectrum excited at 635 nm, so that the S-values can be compared to the location of the broad fluorescence bands identified above.

4. Discussion

As recently summarized [54], EET from PC to Chl *d* in the intact PBP antenna of *A. marina* is generally characterized by four kinetic components with lifetimes of <400 fs, 3 ps, 14 ps and 70 ps at room temperature. An assignment of the latter kinetic components was based on the assumption that the structure of the PBP antenna is similar to one rod of the phycobilisomes in common cyanobacteria. The main difference is that in PBPs of *A. marina* the hexamer closest to the thylakoid membrane is a hetero-hexamer consisting of a PC- and a APC-trimer [8]. The fast <400 fs component was then assigned to an EET process from the α84 to the β84 chromophore within PC trimers of the PBP antenna [16,54]. This is also in agreement with previous reports for PC trimers of other cyanobacteria [56,57]. The 3 ps component was found to originate from the equilibration of the excitation energy between all the PC-hexamers and the APC-molecules of the PC/APC hetero-hexamer. The 14 ps component is observed in the decay associated spectra of the

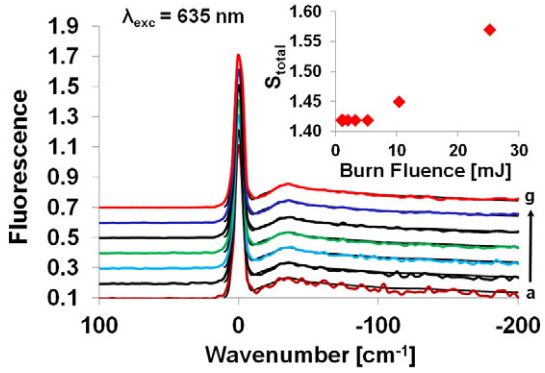

Fig. 6. ΔFLN spectra of phycobiliproteins (noisy curves) and their fits according to Eq. (1) (smooth lines) obtained with an excitation wavelength of 635 nm at 4.5 K at several different burn fluences of a) 1, b) 1.2, c) 2, d) 3.2, e) 5.2, f) 10.4, and g) 25 mJ/cm^2, respectively. The read resolution was 4 cm^{-1}. The ZPLs of all spectra are cut off for clarity. The inset shows the total Huang–Rhys factor S as a function of burn fluence obtained from fits of the fluence-dependent ΔFLN spectra (see Table 2 for parameters).

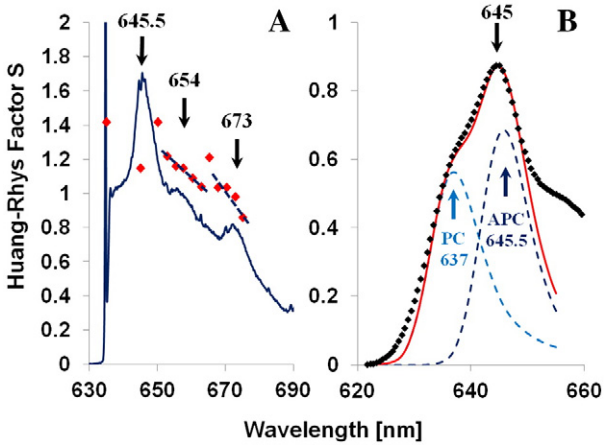

Fig. 7. Frame A: Wavelength-dependence of total Huang–Rhys factor S as given in Table 2. The pre-burn FLN spectrum (blue) of phycobiliproteins obtained with an excitation wavelength of 635 nm at 4.5 K (see Fig. 2) is given for comparison. Broad fluorescence bands unaffected by line-narrowing are labelled by bold arrows and their spectral position in wavelengths. Dashed lines are given as a guide to the eye in order to indicate the wavelength dependence of S within the 654 and 673 nm-bands. Frame B: Fit of the main fluorescence bands of PBP complexes with a PC and an APC component, where each band is described according to Eq. (1) convoluted with a Gaussian IDF with a width (FWHM) of 200 cm^{-1}, see text for details.

transient absorption changes as a decay of a bleaching at 640 nm and a rise of a bleaching at 670 nm. Therefore, this component was assigned to an EET from APC absorbing at about 640 nm to a low energy electronic state associated with the terminal emitter. Our FLN and ΔFLN data provide complementary information on the low-energy level structure of PBPs at 4.5 K as well as on electron–phonon and on electron-vibrational coupling strengths, which determine the homogeneously broadened lineshape of the low-energy states of PBPs of the cyanobacterium *A. marina*. Although data obtained in time-resolved experiments at room temperature and results from line-narrowed spectroscopy at cryogenic temperatures cannot be directly compared, it has been

Table 2
Huang–Rhys factors and parameters of the one-phonon profiles used to fit the 4.2 K ΔFLN spectra of PBP of *A. marina*. The columns corresponding to the ΔFLN spectra shown in Fig. 9 are highlighted in grey.

Excitation Wavelenght [nm]	635	645	650	652.8	655.3	657.5	660.2	662.8	665.2	667.7	670.2	672.8	675
S_{total}	1.42	1.15	1.42	1.22	1.16	1.15	1.09	1.04	1.21	1.035	1.035	0.98	0.86
Uncertainty ΔS	0.1	0.12	0.14	0.12	0.12	0.12	0.12	0.14	0.16	0.14	0.14	0.16	0.16
Profile 1													
Huang–Rhys factor S	0.156	0.12	0.126	0.139	0.125	0.12	0.124	0.11	0.122	0.125	0.11	0.102	0.09
Peak phonon frequency ω_m [cm^{-1}]	35	28	30	35	35	35	35	35	35	35	37	37	37
FWHM of Gaussian wing Γ_G [cm^{-1}]	20	15	15	20	20	20	20	20	20	20	20	20	20
FWHM of Lorentzian wing Γ_L [cm^{-1}]	20	20	15	20	20	20	20	20	10	15	10	10	10
Profile 2													
Huang–Rhys factor S	1.22	1	1	1.05	1	1	0.96	0.9	0.9	1.05	0.9	0.85	0.75
Peak phonon frequency ω_m [cm^{-1}]	20	20	25	20	20	20	20	20	20	20	20	20	20
FWHM of Gaussian wing Γ_G [cm^{-1}]	25	25	25	25	25	25	25	25	25	25	25	25	25
FWHM of Lorentzian wing Γ_L [cm^{-1}]	160	140	120	160	160	140	140	160	120	100	90	90	160
Profile 3													
Huang–Rhys factor S	0.043	0.03	0.037	0.031	0.036	0.03	0.0143	0.03	0.026	0.031	0.025	0.025	0.022
Peak phonon frequency ω_m [cm^{-1}]	134	115	115	134	134	134	134	115	115	115	115	115	115
FWHM of Gaussian wing Γ_G [cm^{-1}]	20	20	20	20	20	20	20	20	20	20	20	20	20
FWHM of Lorentzian wing Γ_L [cm^{-1}]	60	60	60	60	60	40	40	60	30	30	20	20	20

shown before that temperature decrease mainly slows down EET kinetics, while the overall features of EET remain intact [58,59].

4.1. Low-energy (fluorescent) states

A minimum of two fluorescent states roughly located at 636 and 645 nm can be deduced from the dual maximum of the non-line-narrowed fluorescence spectrum of PBP in 70% glycerol at 4.2 K and its second derivative shown in Fig. 1. Based on a comparison to literature data (see Theiss et al. [54] and references therein), the two fluorescence bands can be tentatively associated with the lowest energy levels of PC and APC, respectively, while an apparent heterogeneity among PC subunits identified in recent biochemical analyses of PBPs [60] may also play a role. The position of the lowest energy level of APC at about 645 nm is further corroborated by the presence of a broad fluorescence band at that position in the pre-burn FLN spectrum excited at 635 nm. The 645 nm-band is also in good agreement with the absorption maximum of APC of *A. marina* at about 640 nm reported by Hu et al. [9]. A more precise assignment of the two aforementioned low-energy states requires e.g. constant-fluence hole burning experiments. Such studies are under way and will be discussed elsewhere.

Assuming a rod-shaped structure of PBPs of three homo-hexamers of PC and one hetero-hexamer of PC/APC, the above assignment of two low-energy states to the lowest energy levels of PC and APC, respectively, appears reasonable. However, it is remarkable, that the series of pre-burn FLN spectra excited across the complete spectral range of the non-line-narrowed fluorescence spectrum of Fig. 1 reveals the existence of three further electronic states populated by EET, which are located at about 654, 659, and 673 nm, respectively. That is, these electronic states are found lower in energy than the absorption band of APC at about 640 nm [9]. However, in the same study [9] PBP-PS II complexes showed – among others – one fluorescence band at about 665 nm at 77 K that was also attributed to APC. Assuming a reasonable Stokes shift in the order of 1–2 nm (for a review, see ref. [18]), it is likely that the 659 nm band observed here is responsible for the latter 665 nm fluorescence (see below for a more precise discussion of the Stokes shift involving parameters of electron–phonon coupling determined within this study). At a first glance, however, the assignment of the two fluorescence bands at 636 nm and 645 nm observed in PBP in 70% glycerol at 4.2 K to the lowest-energy states of PC and APC, respectively, appears to be in contradiction to previous results of refs. [12] and [61]. In the latter studies, 77 K decay associated spectra and a room temperature non-line-narrowed fluorescence spectrum revealed broad fluorescence bands at 640 and 665 nm that were assigned to PC and APC, respectively. However, it has to be kept in mind that the latter measurements cannot provide the resolution of a spectrally selective technique like FLN and employed a broad band optical filter to reject excitation laser light at 635 nm so that a fluorescence band at this position could not be detected in the latter studies. Therefore, it can be concluded that the 640 nm band of refs. [12] and [61] most likely corresponds to the 644.5 nm band reported on here or to the envelope of both, the 636 and the 644.5 nm bands. Then, the second, rather broad 665 nm fluorescence band of refs. [12] and [61] would reflect the integrated 654, 659, and 673 nm fluorescence bands resolved by FLN spectroscopy here.

The above assignment of low-energy states is also in qualitative agreement with recent results of both, fs-absorption spectroscopy [16] and time-resolved fluorescence spectroscopy [61]. At room temperature, fs-absorption spectroscopy [16] revealed a fast sub-picosecond EET from 618 nm to ~630 nm almost coincident with the 629 nm-absorption band. This step is followed by slower EET to states at ~648 nm in the vicinity of the second fluorescence band at ~645 nm and eventually to the terminal emitter at ~670 nm, which is roughly coincident with broad fluorescence band at 673 nm. Note in this regard that excitonic states in pigment-protein complexes may exhibit temperature-dependent spectral shifts in the range of several nanometers [62,63].

However, to the best of our knowledge, the fluorescence bands at 654 and 659 nm have not been reported before for PBPs of *A. marina*. In summary, this means that our data indicate the presence of a total of five different fluorescent states spread over a broad spectral range, which are located at 635 (PC), 645 nm (APC), 654, 659 and 673 nm in PBPs at cryogenic temperatures. The observation of five different fluorescent states indicates that in some of the PBPs in the bulk solution EET is impaired in preparations containing 70% glycerol. The finding of a broad fluorescence band at ~673 nm shows that at least some PBPs in the bulk solution remain intact and exhibit EET to the terminal emitter, which is as far as ~30 nm to the red of the major fluorescence bands at 635 and 643 nm. The observation of the four other fluorescence bands suggests that EET is impaired in subsets of the PBPs under study. This finding is in line with results of time-resolved fluorescence experiments on PBP in glycerol revealing an interrupted EET to the terminal emitter at ~670 nm, which was attributed to a partial dissection of the PC and APC subunits of PBP [61]. This means in more detail, that some of the rod-shaped PBPs terminate with PC, some with APC, while at least three further types of PBPs with different emitting states have to be inferred when searching for a structural assignment of the three lowest energy electronic states observed within this study.

The only further structural unit present in PBPs is the linker protein. However, it is impossible to associate all three remaining low-energy states with a single protein complex, because a dissection into the structural components would not lead to three terminal states within one and the same constituent of the PBP rod, which are spectrally widely separated and should thus still be connected via EET. This situation is clearly different from the observation of two quasi-resonant low-energy states within one and the same complex in case of CP43 [29]. In this context, it is interesting to note that recent biochemical analyses of similar PBP preparations as studied here by S. Hildebrandt [60] has revealed the possible presence of three different forms of linker proteins with molecular masses of approximately 32, 35 and 38 kDa, respectively. These putative types of linker proteins are visible as distinct bands in SDS polyacrylamide gels using the method reported by Raps (see Fig. 8 and refs. [47] and [60]) and at least one of them has been unambiguously identified by partial sequence analysis after in gel digestion with trypsin by nano-LC–ESI–MS/MS (Uniprot code: A8ZMJ1, see refs. [48] and [60]). It is reasonable to assume that PCB molecules bound to these three different forms of coloured linker proteins may exhibit different absorption maxima due to a different protein microenvironment. Furthermore it should be mentioned that at least two different types of the α-subunit and at least two different types of the ß-subunit of PC were detected and related to the respective gene sequences (Uniprot code: A8ZMJ1, see ref. [60]), while APC could not be identified by mass spectrometric analysis. In summary, it appears that heterogeneity

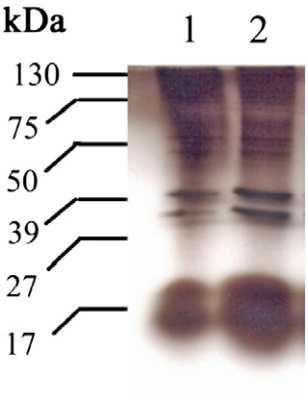

Fig. 8. SDS-PAGE of two different samples of PBP preparations labelled by their molecular mass in kDa according to comigration of marker proteins (left scale). While the bands around 17 kDa correspond to PBPs, there are three further bands close to a molecular mass of 39 kDa indicating the presence of an additional group of proteins, see text.

among the structural components of the PBP rods is responsible for the observed five low-energy fluorescence bands of PBP, while a precise structural assignment of the latter bands requires further studies on isolated components.

4.2. Electron-vibrational coupling

The ΔFLN spectra of *A. marina* obtained in this study reveal a rich vibrational structure, which is characteristic of the pigment molecules bound by PBPs (see Figs. 2–5 and Table 1). The obtained frequencies were compared with the resonance Raman spectra of phycocyanobilin (PCB) in recombinant phytochrome (Table 1), i.e. the same chromophore but embedded into a different protein matrix [64]. In the range of H-out-of-plane-wagging modes (~800 cm^{-1}) and N–H– and C–H-rocking modes (~1300 cm^{-1}), there is only a qualitative agreement of the observed vibrational frequencies, which is most probably due to the different protein environment in PBP complexes. In particular, PBPs exhibit vibronic bands at 723 and 834 cm^{-1}, respectively, in the region of H-out-of-plane wagging modes. PBPs also show vibronic bands at 1246, 1273 and 1363 cm^{-1}, respectively, in the region of N–H and C–H rocking modes. Two intense modes are observed at ~1634 and ~1580 cm^{-1}, respectively, which are characteristic of the PCB pigment. The mode at 1580 cm^{-1} corresponds to a CNH^{+} stretching motion (see inset of Fig. 2) [64]. The vibronic band at 1634 cm^{-1} represents a C_{19}–C_{20} stretching mode (see inset of Fig. 2) [64]. The vibronic structure of PBPs obtained at different excitation wavelengths is compared in Fig. 9. Overall, the vibrational frequencies obtained at different excitation wavelengths are rather similar (see Table 1 and Fig. 9). The excitation wavelengths of the ΔFLN spectra shown in Fig. 9 do roughly correspond to the peak wavelengths of four of the above identified electronic states. Some of the PBP vibrational modes appear to be slightly shifted depending on excitation wavelength indicating that the particular protein environment of individual pigment molecules may tune the vibrational frequencies. Nevertheless, the finding of rather similar vibronic modes for all identified electronic states suggests that the same type of pigment molecule, i.e. PCB, is responsible for the five fluorescent electronic states assigned above.

The $S_1 \rightarrow S_0$ vibrational frequencies of PBP obtained here are compared with those of Chl *a*-WSCP [65,66] in Table 1 and in Fig. 9. A comparison of the data reveals that several intense characteristic modes of Chl *a*, e.g. 742, 1184, 1217, 1329, and 1532 cm^{-1} [65,66], are missing in the PBP spectra so that the PBPs under study should be virtually free of Chl *a*. Regardless of this finding, a few PBP modes listed in Table 1 do also appear in the Chl *a* spectra. This is probably related to similar structural motifs. Both, Chl a and PCB, are tetrapyrrole molecules

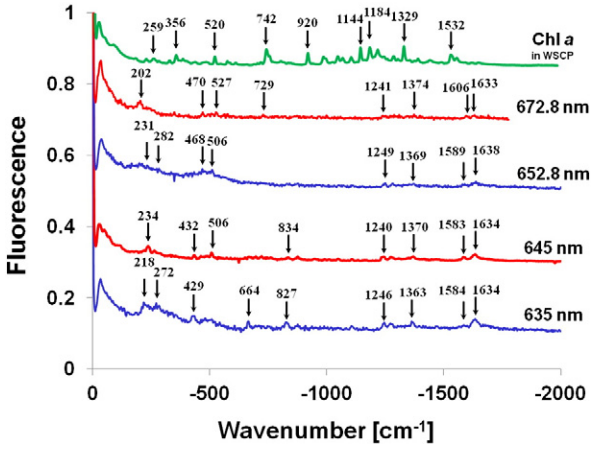

Fig. 9. Vibronic region of PBP ΔFLN spectra obtained with excitation wavelengths of 635, 645, 652.8, and 672.8 nm applying a burn fluence of 25 mJ/cm^2 at 4.5 K. The ZPLs of both spectra are cut off at 60% of their peak intensity for clarity. Distinct vibrational lines are marked by thin arrows and their frequencies in wavenumbers, see Table 1.

with the latter being a linear chain of four pyrrol rings with a larger flexibility than the planar Chl molecule. Vibrations in the 200–600 cm^{-1} range are typically associated with a variety of collective vibrational motions of the tetrapyrrole backbone of Chl, while frequencies higher than 1000 cm^{-1} mainly represent motions of individual molecular groups like e.g. the C=O stretching mode typically found in the range of ~1700 cm^{-1} [67]. Thus, the observation of similar vibrational frequencies may suggest that the lower-frequency modes in the 200–600 cm^{-1} range are restricted to collective motions within individual pyrrol rings. In addition, there are two Chl *a* frequencies at ~1591 and 1620 cm^{-1} [65,66], respectively, which are very close to the two characteristic modes of PCB discussed above. Nevertheless, a close inspection of Fig. 9 reveals that the vibronic structures observed for PBPs and for Chl *a* are essentially different so that it appears reasonable to attribute the observed low-energy states in PBP to PCB molecules.

4.3. Electron–phonon coupling

ΔFLN spectra were measured at several wavelengths within the fluorescence origin bands ranging from ~ 635 up to 675 nm. All identified electronic states at 635 (PC), 645 (APC), 654, 659, and 673 nm, respectively, are characterized by different S-factors and – in part – by different mean phonon frequencies and/or one phonon profiles characterizing the individual pigment-protein interaction and the specific protein environment, respectively, see Table 2. The observed S-factors fall in the range from S = 0.89 (terminal emitter) to S = 1.42 (PC) consistent with moderate electron–phonon coupling. The phonon frequencies ω_m vary from 31 cm^{-1} (645 nm, APC) to 37 cm^{-1} (672.8 nm, terminal emitter) and are thus among the highest peak frequencies reported for protein phonons in the literature (see Table 3 for a comparison). Both, the moderate to large electron–phonon coupling strengths S and the relatively high phonon frequencies obtained for PBP should lead to relatively large Stokes-shifts $2S\omega_m$ or reorganization energies $S\omega_m$, where the latter represents the shift between the fluorescence bands observed here and the corresponding 0–0-transitions. However, it has to be kept in mind that the above approximations may overestimate the real values especially in cases of broad and asymmetric one-phonon profiles as observed for PBPs in this study. Based on the values summarized in Table 2, the reorganization energies $S\omega_m$ should reach upper limits of 49 cm^{-1} (~2 nm) for PC (635 nm) and 32 cm^{-1} (~1.5 nm) for APC (645 nm). The latter value for APC is too small to assign a fluorescence band at 665 nm [9,12,61] to an absorption band at about 640 nm [9] or 644.5 nm (this study). In order to verify the parameters of electron–phonon coupling determined above, we have calculated the main fluorescence band of PBP complexes peaking at about 645 nm (see Fig. 1) assuming two bands corresponding to PC and APC, respectively, where each band is described by Eq. (1) convoluted with a Gaussian IDF with a width (FWHM) of 200 cm^{-1} and the S-factors and one-phonon profiles determined for 635 nm (PC) and 645 nm (APC), respectively (see Table 2). The spectral positions of the electronic 0–0 transitions were treated as free parameters. The resulting fit shown in Frame B of Fig. 7 has a reasonable agreement with the measured spectrum and reproduces its peak position. The peak positions of the fluorescence bands are ~637 nm (PC) and ~645.5 nm (APC), where the latter is in very good agreement with the broad band observed in the pre-burn FLN spectrum excited at 635 nm (see Fig. 2). The resulting peak positions of the corresponding electronic 0–0 transitions are ~635.1 nm (PC) and ~644.5 nm (APC) coincident with the respective shoulder in the 4.5 K absorption spectrum. Thus, the observed displacements are 1.9 and 1.0 nm for PC and APC, respectively, which is in general agreement with the reorganization energies mentioned above. As theoretically expected, the larger S-factor and larger mean phonon frequency determined for PC leads to larger reorganization energy. Furthermore, the reorganization energy determined for APC appears to be in good agreement with the observed peak positions of APC in absorption and fluorescence/FLN. Nevertheless, an accurate assignment of the

Table 3
Mean phonon frequencies ω_m and one-phonon profiles l_1 obtained for different photosynthetic pigment–protein complexes assuming a Gaussian and Lorentzian lineshape at the low- and high-energy side of the mean phonon frequency ω_m.

Complex	Mean phonon frequency ω_m, cm^{-1}	FWHM of the Gaussian wing of the one-phonon profile l_1, cm^{-1}	FWHM of the Lorentzian wing of the one-phonon profile l_1, cm^{-1}	Reference
PBP of *A. marina*	31–37	25	90–160	This study
FMO from green sulphur bacteria	21	21	56	Rätsep and Freiberg [21]
LH1 from *Rb. sphaeroides*	26	26	130	Freiberg et al. [69]
B850 band of LH2 from *Rb. sphaeroides*	28	28	80	Freiberg et al. [69]
CP29	22	20	130	Rätsep et al. [39]
LHC II trimer	18	16	160	Pieper et al. [70]
Chl *a* dimers in WSCP[1]	24			Pieper et al. [65]

[1] A proper description of the highly structured PSB of WSCP delta-FLN spectra required the assumption of three individual one-phonon profiles, Pieper et al. [65] for details.

fluorescent states requires the determination of the location of the inhomogeneously broadened 0–0 transition profiles by constant fluence hole-burning spectroscopy. Such experiments are in progress.

It is known that the linear electron–phonon coupling strength S may strongly vary with excitation wavelength across the inhomogeneously broadened absorption band. An almost linear increase of S with increasing excitation wavelength has been reported e.g. for isolated Chl *a* [51] and Bchl *a* [68] molecules as well as for the antenna complexes CP29 of green plants [39], LH1 and LH2 [69] suggesting a strong correlation between the electron–phonon coupling strength and the solvent shift. However, the opposite tendency, i.e. a decrease of S with increasing excitation wavelength has also been reported for some pigment-protein complexes such as FMO [21] and WSCP [65]. The latter dependence was attributed to efficient energy transfer from a higher excitonic state overlapping the fluorescent state at the blue side of the inhomogeneously broadened fluorescence band. The wavelength-dependence of the S-factors determined for PBP is plotted along with the pre-burn FLN spectrum excited at 635 nm in Fig. 7 A. S-factors of 1.42 and 1.15 were obtained at 635 and 645 nm corresponding to the fluorescence bands of PC and APC, respectively, see above. Thus, only one S-factor is available characterizing the electron–phonon coupling strength for these two low-energy states. For the two fluorescence bands at 654 and 673 nm, however, the S-factor seems to become smaller with increasing wavelength as observed before for the FMO complex and WSCP. This effect may be an intrinsic feature of the 654 and 673 nm-fluorescence bands. In case of the 654 nm-band, however, it is possible that this dependence originates from overlap with the closely spaced 659 nm-band (visible in Fig. 4) assuming different S-factors for those bands. On the other hand, it cannot be ruled out that there is only an apparent increase of S at the blue side of both bands due to efficient EET from overlapping higher energy states as inferred for WSCP [65].

5. Conclusion

High-resolution, spectrally selective FLN and ΔFLN spectroscopy has been employed to study excitation energy transfer, electron–phonon, and electron-vibrational coupling in PBPs of *A. marina* at 4.5 K. A total of five low-energy electronic states with fluorescence bands located at ~635 nm (PC), 645 nm (APC), 654 nm, 659 nm and a terminal emitter at about 673 nm can be resolved within the structure less red tail of the absorption spectrum of PBPs. The spectral heterogeneity can be associated with isoforms of the PC subunits and/or three different isoforms of the linker protein having apparent molecular weights of 32, 35 and 38 kDa. However, further experiments on isolated subunits are necessary to verify this conclusion. The electron–phonon coupling parameters are found to vary significantly with electronic state, thus reflecting the different protein environments of the respective pigment molecules. PBPs exhibit remarkably high mean phonon frequencies up to 37 cm^{-1} and moderate to large Huang–Rhys factor S between 0.98 (terminal emitter), 1.15 (APC), and 1.42 (PC). Two characteristic vibronic lines of C–NH^+ and C–C stretching modes, respectively, indicate that all electronic states observed are due to PCB chromophores.

Acknowledgement

Financial Support by the Estonian Science Foundation (Grant No. 9453) and the Estonian Research Council (Grant IUT02-28) is gratefully acknowledged. J. P. is also deeply indebted to the European Social Fund's Internationalisation Programme DoRa for financial support. Furthermore, J.P., and H.-J.E. gratefully acknowledge support from Deutsche Forschungsgemeinschaft (SFB 429, TP A1). We also thank S. Kussin and M. Weß (TU Berlin) for their expert help in sample preparation.

References

[1] A.R. Grossman, D. Bhaya, K.E. Apt, D.M. Kehoe, Light-harvesting complexes in oxygenic photosynthesis: diversity, control, and evolution, Annu. Rev. Genet. 29 (1995) 231–288.
[2] R.M. Clegg, M. Sener, Govindjee From Förster resonance energy transfer (FRET) to coherent resonance energy transfer (CRET) and back, Proc. SPIE 7561 (2010) 7561–7612.
[3] R. Blankenship, Govindjee, Photosynthesis, The Encyclopedia of Science and Technology, 10th edition13, 2007. 468–475.
[4] H. Miyashita, H. Ikemoto, N. Kurano, K. Adachi, M. Chihara, S. Miyachi, Chlorophyll d as a major pigment, Nature 383 (1996) 402.
[5] A.W.D. Larkum, M. Kühl, Chlorophyll d: the puzzle resolved, Trends Plant Sci. 10 (8) (2005) 355.
[6] M. Chen, R.G. Quinnell, A.W.D. Larkum, The major light-harvesting pigment protein of *Acaryochloris marina*, FEBS Lett. 514 (2002) 149–152.
[7] M. Chen, T.S. Bibby, Photosynthetic apparatus of antenna-reaction centres supercomplexes in oxyphotobacteria: insight through significance of Pcb/IsiA proteins, Photosynth. Res. 86 (2005) 165–173.
[8] J. Marquardt, H. Senger, H. Miyashita, S. Miyachi, E. Mörschel, Isolation and characterization of biliprotein aggregates from *Acaryochloris marina*, a prochloron-like prokaryote containing mainly chlorophyll d, FEBS Lett. 410 (1997) 428–432.
[9] Q. Hu, J. Marquardt, I. Iwasaki, N. Miyashita, H. Kurano, E. Mörschel, S. Miyachi, Molecular structure localization and function of biliproteins in the chlorophyll a/d containing oxygenic photosynthetic procaryote *Acaryochloris marina*, Biochim. Biophys. Acta 1412 (1999) 250–261.
[10] J. Marquardt, E. Mörschel, E. Rhiel, M. Westermann, Ultrastructure of *Acaryochloris marina*, an oxyphotobacterium containing mainly chlorophyll d, Arch. Microbiol. 174 (2000) 181–188.
[11] M. Chen, M. Floetenmeyer, T.S. Bibby, Supramolecular organization of phycobiliproteins in the chlorophyll d-containing cyanobacterium *Acaryochloris marina*, FEBS Lett. 583 (2009) 2535–2539.
[12] Z. Petrasek, F.J. Schmitt, C. Theiss, J. Huyer, M. Chen, A. Larkum, H.J. Eichler, K. Kemnitz, H.-J. Eckert, Excitation energy transfer from phycobiliprotein to chlorophyll d in intact cells of *Acaryochloris marina* studied by time- and wavelength-resolved fluorescence spectroscopy, Photochem. Photobiol. Sci. 12 (2005) 1016–1022.
[13] N. Adir, Elucidation of the molecular structures of components of the phycobilisome: reconstructing a giant, Photosynth. Res. 85 (2005) 15–32.
[14] R. Mac Coll, Allophycocyanin and energy transfer, Biochim. Biophys. Acta 1657 (2004) 73–81.
[15] M. Watanabe, M. Ikeuchi, Phycobilisome: architecture of a light-harvesting supercomplex, Photosynth. Res. 116 (2–3) (2013) 265–276.
[16] C. Theiss, F.J. Schmitt, S. Andree, C. Cardenas-Chavez, K. Wache, J. Fuesers, M. Vitali, M. Wess, S. Kussin, H.J. Eichler, H.-J. Eckert, Excitation energy transfer in the phycobiliprotein antenna of *Acaryochloris marina* studied by transient fs absorption and fluorescence spectroscopy, Photosynthesis: energy from the sun, 14th International Congress on Photosynthesis, Springer, Dordrecht, 2008, pp. 339–342.

[17] R. Purchase, S. Völker, Spectral hole burning: examples from photosynthesis, Photosynth. Res. 101 (2009) 245–266.
[18] R. Jankowiak, M. Reppert, V. Zazubovich, J. Pieper, T. Reinot, Site selective and single complex laser-based spectroscopies: a window on excited state electronic structure, excitation energy transfer, and electron–phonon coupling of selected photosynthetic complexes, Chem. Rev. 8 (2011) 4546–4598.
[19] R. Jaaniso, Determination of homogenous spectra and the inhomogeneous distribution function by hole burning method, Proc. Acad. Sci. Estonian SSR Phys. Math. 34 (1985) 277–283.
[20] J. Fünfschilling, D. Glatz, I. Zschokke-Gränacher, Hole-burning spectroscopy as a tool to eliminate inhomogeneous broadening, J. Lumin. 36 (1986) 85–92.
[21] M. Rätsep, A. Freiberg, Electron–phonon and vibronic couplings in the FMO bacteriochlorophyll a antenna complex studied by difference fluorescence line narrowing, J. Lumin. 127 (2007) 251–256.
[22] M. Rätsep, R.E. Blankenship, G.J. Small, Energy transfer and spectral dynamics of the three lowest energy Qy-states of the Fenna–Matthews–Olson antenna complex, J. Phys. Chem. B 103 (1999) 5736–5741.
[23] T.M.H. Creemers, C.A. De Caro, R.W. Visschers, R. van Grondelle, S. Völker, Spectral hole burning and fluorescence line-narrowing in subunits of the light-harvesting complex LH1 of purple bacteria, J. Phys. Chem. B 103 (1999) 9770–9776.
[24] J. Pieper, K.-D. Irrgang, M. Rätsep, J. Voigt, G. Renger, G.J. Small, Assignment of the lowest Qy-state and spectral dynamics of the CP29 chlorophyll a/b antenna complex of green plants: a hole-burning study, Photochem. Photobiol. 71 (2000) 574–581.
[25] J. Pieper, M. Rätsep, R. Jankowiak, K.-D. Irrgang, J. Voigt, G. Renger, G.J. Small, Q(y)-level structure and dynamics of solubilized light-harvesting complex II of green plants: pressure and hole burning studies, J. Phys. Chem. A 103 (1999) 2412–2421.
[26] J. Friedrich, H. Scheer, B. Zickendraht-Wendelstadt, D. Haarer, Energy transfer in phycobiliproteins as studied by photochemical hole burning, J. Lumin. 24/25 (1981) 815–818.
[27] N.R.S. Reddy, R. Picorel, G.J. Small, B896 and B870 components of the *Rhodobacter sphaeroides* antenna: a hole burning study, J. Phys. Chem. 96 (1992) 6458–6464.
[28] H.-M. Wu, M. Rätsep, R. Jankowiak, R.J. Cogdell, G.J. Small, Comparison of the LH2 antenna complexes of *Rhodopseudomonas acidophila* (Strain 10050) and *Rhodobacter sphaeroides* by high-pressure absorption, high-pressure hole burning, and temperature-dependent absorption spectroscopies, J. Phys. Chem. B 101 (1997) 7641–7654.
[29] V. Zazubovich, R. Jankowiak, On the energy transfer between quasi-degenerate states with uncorrelated site distribution functions: an application to the CP43 complex of photosystem II, J. Lumin. 127 (2007) 245–250.
[30] B. Neupane, N.C. Dang, K. Acharya, M. Reppert, V. Zazubovich, R. Picorel, M. Seibert, R. Jankowiak, Insight into the electronic structure of the CP47 antenna protein complex of photosystem II: hole burning and fluorescence study, J. Am. Chem. Soc. 132 (2010) 4214–4229.
[31] H.-C. Chang, G.J. Small, R. Jankowiak, Temperature dependent hole burning of the 684 nm chlorophyll a of the isolated reaction center of photosystem II: confirmation of the linker model, Chem. Phys. 194 (1995) 323–333.
[32] F.T.H. den Hartog, J.P. Dekker, R. van Grondelle, S. Völker, Spectral distributions of 'trap' pigments in the RC, CP47, and CP47-RC complexes of photosystem II at low temperature: a fluorescence line-narrowing and hole-burning study, J. Phys. Chem. B 102 (1998) 11007–11016.
[33] J. Pieper, J. Voigt, G. Renger, G.J. Small, Analysis of phonon structure in line-narrowed optical spectra, Chem. Phys. Lett. 310 (1999) 296–302.
[34] J.M. Hayes, S. Matsuzaki, M. Rätsep, G.J. Small, Red chlorophyll a antenna states of photosystem I of the *Cyanobacterium Synechocystis* sp. PCC 6803, J. Phys. Chem. B 104 (2000) 5625–5633.
[35] J.L. Hughes, R. Picorel, M. Seibert, E. Krausz, Photophysical behavior and assignment of the low-energy chlorophyll states in the CP43 proximal antenna protein of higher plant photosystem II, Biochemistry 45 (2006) 12345–12357.
[36] J.K. Gillie, G.J. Small, J.H. Golbeck, Nonphotochemical hole burning of the native antenna complex of photosystem I (PSI-200), J. Phys. Chem. 93 (1989) 1620–1627.
[37] V. Zazubovich, I. Tibe, G.J. Small, Bacteriochlorophyll a Franck–Condon Factors for the $S_0 \rightarrow S_1$ (Qy) transition, J. Phys. Chem. B 105 (2001) 12410–12417.
[38] M. Rätsep, A. Freiberg, Resonant emission from the B870 exciton state and electron–phonon coupling in the LH2 antenna chromoprotein, Chem. Phys. Lett. 377 (2003) 371–376.
[39] M. Rätsep, J. Pieper, K.-D. Irrgang, A. Freiberg, Excitation wavelength-dependent electron–phonon and electron-vibrational coupling in the CP29 antenna complex of green plants, J. Phys. Chem. B 112 (2008) 110–118.
[40] J. Pieper, M. Rätsep, K.-D. Irrgang, A. Freiberg, Chromophore–chromophore and chromophore–protein interactions in monomeric light-harvesting complex II of green plants studied by spectral hole burning and fluorescence line narrowing, J. Phys. Chem. B 113 (2009) 10870–10880.
[41] J. Friedrich, H. Scheer, B. Zickendraht-Wendelstadt, D. Haarer, Photochemical hole burning: a means to observe high resolution optical structures in phycoerythrin, J. Chem. Phys. 74 (1981) 2260–2266.
[42] J. Friedrich, H. Scheer, B. Zickendraht-Wendelstadt, D. Haarer, High-resolution optical studies on C-phycocyanin via photochemical hole burning, J. Am. Chem. Soc. 103 (1981) 1030–1035.
[43] W. Köhler, J. Friedrich, R. Fischer, H. Scheer, Site-selective spectroscopy and level ordering in C-phycocyanin, Chem. Phys. Lett. 143 (1988) 169–173.
[44] M. Chen, T.S. Bibby, J. Nield, A.W.D. Larkum, J. Barber, Structure of a large photosystem II supercomplex from *Acaryochloris marina*, FEBS Lett. 579 (2005) 1306–1310.
[45] U. Laemmli, Cleavage of structural proteins during the assembly of the head of bacteriophage T4, Nature (London) 227 (1970) 680–685.
[46] H. Blum, H. Beier, H.J. Gross, Improved silver staining of plant proteins, RNA and DNA in polyacrylamide gels, Electrophoresis 8 (1987) 93–99.
[47] S. Raps, Differentiation between phycobiliproteins and colorless linker polypeptides by fluorescence in the presence of ZnSO4, Plant Physiol. 92 (1990) 358–362.
[48] W.D. Swingley, M. Chen, P.C. Cheung, A.L. Conrad, L.C. Dejesa, J. Hao, B.M. Honchak, L.E. Karbach, A. Kurdoglu, S. Lahiri, S.D. Mastrian, H. Miyashita, L. Page, S. Satoh, W.M. Sattley, Y. Shimada, H.L. Taylor, T. Tomo, T. Tsuchiya, Z.T. Wang, J. Raymond, M. Mimuro, R.E. Blankenship, J.W. Touchman, Niche adaptation and genome expansion in the chlorophyll d-producing cyanobacterium *Acaryochloris marina*, Proc. Natl. Acad. Sci. U. S. A. 105 (2008) 2005–2010.
[49] K.S. Rowan, Photosynthetic pigments of algae, Cambridge University Press, Cambridge, 1989. 166–211.
[50] R.J. Richie, Consistent sets of spectrophotometric chlorophyll equations for acetone, methanol and ethanol solvents, Photosynth. Res. 89 (2006) 27–41.
[51] M. Rätsep, J. Linnanto, A. Freiberg, Mirror symmetry and vibrational structure in optical spectra of chlorophyll a, J. Chem. Phys. 130 (2009) 194501.
[52] M. Reppert, V. Naibo, R. Jankowiak, Accurate modeling of fluorescence line narrowing difference spectra: direct measurement of the single-site fluorescence spectrum, J. Chem. Phys. 133 (2010) 1–9.
[53] J.M. Hayes, P.A. Lyle, G.J. Small, A theory for the temperature dependence of hole-burned spectra, J. Phys. Chem. 98 (1994) 7337–7341.
[54] C. Theiss, F.-J. Schmitt, J. Pieper, C. Nganou, M. Grehn, M. Vitali, R. Olliges, H.J. Eichler, H.-J. Eckert, Excitation energy transfer in intact cells and in the phycobiliprotein antennae of the chlorophyll d containing cyanobacterium *Acaryochloris marina*, J. Plant Physiol. 168 (12) (2011) 1473–1487.
[55] A.C. Nganou, On the role of pigment–pigment and pigment–protein interaction in regulating excitation energy and electron transfer in photosynthesis, (PhD thesis) Technical University Berlin, 2012.
[56] T. Gillbro, A. Sharkov, I. Kryukov, E. Khoroshilov, P. Kryukov, R. Fischer, H. Scheer, Forster energy-transfer between neighboring chromophores in C-phycocyanin trimers, Biochim. Biophys. Acta 1140 (1993) 321–326.
[57] M. Debreczeny, K. Sauer, J.H. Zhou, D. Bryant, Comparison of calculated and experimentally resolved rate constants for excitation energy transfer in C-phycocyanin. 2. Trimers, J. Phys. Chem. 99 (1995) 8420–8431.
[58] T. Bittner, K.-D. Irrgang, G. Renger, M.R. Wasilewski, Ultrafast excitation energy transfer and exciton–exciton annihilation processes in isolated light harvesting complexes of photosystem II (LHC II) from spinach, J. Phys. Chem. 98 (1994) 11821–11826.
[59] T. Bittner, G.P. Wiederrecht, K.-D. Irrgang, G. Renger, M.R. Wasilewski, Femtosecond transient absorption spectroscopy on the light-harvesting Chla/b protein complex of Photosystem II at room temperature and 12 K, Chem. Phys. 194 (1995) 311–322.
[60] Hildebrandt, Charakterisierung von Pigment–Proteinkomplexen aus dem Cyanobakterium *Acaryochloris marina*, (Bachelor thesis) University for Applied Sciences, Berlin, Germany, 2009. (in German).
[61] F.J. Schmitt, K. Wache, J. Fuesers, S. Andree, A. Handojo, A. Karradt, D. Kiekebusch, H.J. Eichler, H.-J. Eckert, Investigation of the excited states dynamics in the Chl d-containing cyanobacterium *Acaryochloris marina* by time- and wavelength correlated single-photon counting, Proc. SPIE 6386 (2006) 6386–6387.
[62] J. Pieper, R. Schödel, K. Irrgang, J. Voigt, G. Renger, Electron–phonon coupling in solubilized LHC II complexes of green plants investigated by line-narrowing and temperature-dependent fluorescence spectroscopy, J. Phys. Chem. B 105 (2001) 7115–7124.
[63] H. Rogl, R. Schödel, H. Lokstein, W. Kühlbrandt, A. Schubert, Assignment of spectral substructures to pigment-binding sites in higher plant light-harvesting complex LHC-II, Biochemistry 41 (2002) 2281–2287.
[64] F. Andel, J.T. Murphy, J.A. Haas, M.T. Mc Dowell, I. van der Hoef, J. Lugtenburg, J.C. Lagarias, R.A. Mathies, Probing the photoreaction mechanism of phytochrome through analysis of resonance Raman vibrational spectra of recombinant analogues, Biochemistry 39 (10) (2000) 2667–2676.
[65] J. Pieper, M. Rätsep, I. Trostmann, H. Paulsen, G. Renger, A. Freiberg, Excitonic energy level structure and pigment–protein interactions in the recombinant water-soluble chlorophyll protein. I. Difference fluorescence line-narrowing, J. Phys. Chem. B 115 (14) (2011) 4042–4052.
[66] J. Pieper, M. Rätsep, I. Trostmann, F.-J. Schmitt, C. Theiss, H. Paulsen, A. Freiberg, G. Renger, Excitonic energy level structure and pigment–protein interactions in the recombinant water-soluble chlorophyll protein. II. Spectral hole-burning experiments, J. Phys. Chem. B 115 (14) (2011) 4053–4065.
[67] M. Lutz, Resonance Raman spectra of chlorophyll in solution, J. Raman Spectrosc. 2 (1974) 497–516.
[68] I. Renge, M. Rätsep, A. Freiberg, Intermolecular repulsive–dispersive potentials explain properties of impurity spectra in soft solids, J. Lumin. 131 (2011) 262–265.
[69] A. Freiberg, M. Rätsep, K. Timpmann, G. Trinkunas, Excitonic polarons in quasi-one-dimensional LH1 and LH2 bacteriochlorophyll a antenna aggregates from photosynthetic bacteria: A wavelength-dependent selective spectroscopy study, Chem. Phys. 357 (2009) 102–112.
[70] J. Pieper, K.-D. Irrgang, G. Renger, R.E. Lechner, Density of vibrational states of the light-harvesting complex II of green plants studied by inelastic neutron scattering, J. Phys. Chem. B 108 (2004) 10556–10565.